Observation of Ballistic Phonons in Silicon Crystals Induced by α Particles

B. A. Young, B. Cabrera, and A. T. Lee
Physics Department, Stanford University, Stanford, California 94305
(Received 6 March 1990)

We have observed the ballistic-phonon-focusing pattern along the [100] axis of a 1-mm-thick silicon crystal using α-particle bombardment as the phonon source. These experiments on phonon-mediated particle detection are performed in vacuum at about 400 mK and use titanium-superconducting-transition-edge phonon sensors on the crystal surfaces. The ballistic time of flight is confirmed in one experiment and the focusing patterns are spatially resolved in another. These data indicate that about $\frac{1}{3}$ of the phonon energy striking the back face during the first μsec is ballistic.

PACS numbers: 63.20.−e, 29.40.Ti, 74.75.+t

For insulating crystals such as silicon, the thermal-phonon scattering length exceeds several cm at temperatures below a few kelvins. Because the thermal-phonon density is suppressed at these low temperatures, phonon-phonon interactions are rare, and phonons from an athermal pulse experience only the intrinsic phonon processes of anharmonic decay and isotope scattering. All phonons with frequencies below about 0.5 THz traverse the sample without scattering and are called ballistic.[1] The anisotropic nature of silicon crystals causes a highly anisotropic ballistic-phonon energy transport from a small source within the crystal [see Fig. 4(a) below]. These intricate phonon-focusing patterns reflect the cubic symmetry of the crystal and have been mapped out in great detail with laser-pulse experiments.[2]

Silicon and germanium crystals have been used as particle detectors for many years;[3] however, electron-hole pairs provide the signal in these semiconductor diodes. Recently, our group and others have undertaken the development of phonon-mediated particle detection using silicon crystals.[4] Our group has demonstrated sensitivity to α particles[5] and to x rays.[6] Pröbst *et al.*[7] reported on α-particle experiments with silicon crystals and found suggestions of ballistic-phonon propagation but obtained transition times longer than the ballistic time of flight would suggest. In this paper we report on a new coincidence technique which allows the mapping of the ballistic-focusing patterns and demonstrates that about one-third of the phonon energy flux which traverses our 1-mm crystal from near the α interaction region arrives at the back surface ballistically.

Our experiments use titanium-transition-edge sensors[6,8] (Ti TES), consisting of a 400-Å-thick film of superconducting Ti laid down in a meander pattern on the (100) surface of a 1-mm-thick Si wafer substrate.[9] Each sensor is a series connection of 400 lines (2 μm wide, 5 μm pitch) and is aligned with the [110] axes of the wafer. The resistance of each line just above T_c is ≈ 17 kΩ. Two 4-mm-long by 2-mm-wide sensors lie immediately adjacent to each other and together form a square with active area 16 mm^2. We have developed a technique for aligning these Ti sensors on both the front and back sides of a silicon wafer so that the two meander patterns coincide when viewed along the [100] axis. These multichannel devices have enabled us to perform timing experiments and to obtain spatial information about each event occurring in the detector.

The devices were exposed to a 24-μCi source of ^{241}Am. The decay spectrum of ^{241}Am includes several α lines around ≈ 5.5 MeV, a nuclear γ at 60 keV, and atomic x rays at 18 and 14 keV. In these experiments, however, ^{241}Am was used only as an α source. The α particles have a range of ≈ 25 μm in silicon, with increasing dE/dx towards the end of the track.[10] Three different source-detector geometries were used: F/F, B/B, and F/B, where the labels F for front side and B for back side refer to the location of the detector channels relative to the position of the source.

We use cryogenic GaAs metal-semiconductor field-effect transistor voltage-sensitive preamplifiers with noise $\Delta V_{\rm rms} \approx 1$ nV/$\sqrt{\rm Hz}$ at 1 MHz,[11] and run the detectors in a cryopumped ^{3}He refrigerator that can achieve temperatures down to ≈ 250 mK.[12] We operate at the foot of the resistive transition in temperature ($T_c \approx 430$ mK),[13] and dc current bias the TE devices at a level ($I_{\rm bias} \approx 70$ nA) where self-heating effects are small. A self-terminating voltage pulse (≈ 5 μsec long) results when the film is bombarded with phonons generated by a particle event in the Si crystal substrate. The pulse length is directly related to the phonon escape time from the film (≈ 2 μsec). Ideally, the amplitude of a pulse ($V = I_{\rm bias} \times R$) is simply proportional to the area of the sensor driven normal. In practice, however, the pulse rise time is electronics limited by a slew rate of ≈ 60 kΩ/μsec. For these characteristic frequencies the preamplifier has an effective input impedance $Z_0 \approx 300$ kΩ, which causes a pulse-height suppression for large signals given approximately by $R_{\rm eff} = RZ_0/(R+Z_0)$.[14]

The threshold energy density (E_ρ) necessary to drive a portion of a TE sensor normal may be estimated by integrating the heat capacity (as given by the BCS theory) of the superconductor from the bias temperature to T_c. We assume that the time constants are sufficient to allow quasithermal equilibrium. The asymptotic form of the

surface energy density E_σ given by $E_\rho d$ is

$$E_\sigma \approx 5.0N(0)\Delta_0^2 d[1-T/T_c],$$

where d is the film thickness, Δ_0 is the energy gap at $T=0$, and $N(0)$ is the density of states at the Fermi surface in the normal metal.[15] For our Ti films, $d \approx 400$ Å, $N(0) \approx 4\times 10^{22}$ cm^{-3}eV^{-1}, and $\Delta_0 \approx 47$ μeV, yielding $E_\sigma \approx 0.53$ eV/μm^2 at $T/T_c \approx 0.97$.

In the F/B runs, the α-particle source was collimated with a 150-μm-diam hole cut through 250-μm-thick Mylar. The hole was aligned with the centers of the F and B sensors [see Fig. 1(c)]. Figure 1(a) shows the time-delay data obtained from the leading edges of the front-side and back-side coincident signals for several temperatures. The point size is an estimate of the time uncertainty due to the finite energy spread of the collimated α source ($\approx 15\%$ FWHM), as well as the systematic errors which enter into the analysis as a result of the slightly different operating characteristics of the F and B sensors. By comparison, the statistical errors of ≤ 1 nsec are small. There exists a minimum temperature (≈ 385 mK for this film) below which the Ti film is not sufficiently sensitive to "see" α events through the 1-mm-thick crystal. The local energy density which initiates a signal at this threshold temperature is $E_\sigma \approx 2.5$ eV/μm^2, as given above. This value of E_σ is approximately 5 times greater than that expected for a 1-mm-thick, purely isotropic medium, indicating that substantial phonon focusing occurs within the crystal.

The ballistic-phonon travel time along the [100] axis of silicon is ≈ 168 nsec/mm, and is given by the speed of sound for transverse phonons (the faster, longitudinal phonons have a much smaller intensity). The delay time which corresponds to ballistic propagation in our detector is shown in Fig. 1(a) as a ≈ 4 nsec wide band, which reflects the distribution of α interaction depths within our detector. The ballistic phonons provide the signal onset when operating our detector near T_c. At lower temperatures, however, the ballistic component alone is no longer sufficient to initiate a superconducing-to-normal transition, and diffusive phonons which arrive later begin to significantly contribute to the signal.[16] This accounts for the observed shift to larger time delays for the coincident F/B signals at temperatures ≈ 15 mK below T_c.

For both the F/F and B/B runs, the α source was collimated using a 250-μm-thick Mylar mask which contained a 125-μm-wide slit. The slit was placed perpendicular to the boundary between the two Ti sensors, and to first order irradiated the two channels equally [see Fig. 2(f)]. Figures 2(a)–2(e) show the temperature variation of the B/B pulse-height distribution obtained for coincident signals in two adjacent channels on the back side of the detector. Each point corresponds to an event which exceeded threshold in both channels within an 800-nsec window. Ideally, for a given threshold, events of constant total energy form a straight line of slope -1. However, the data also show a radial distribution of events at each temperature. This distribution

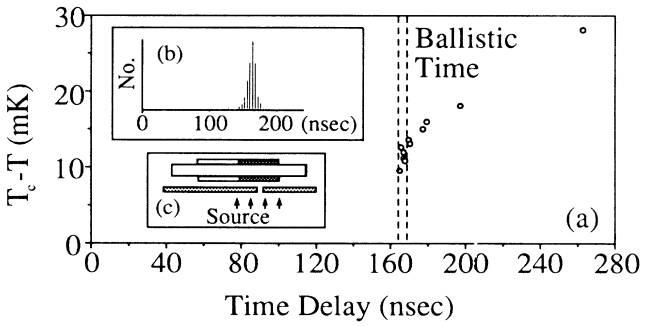

FIG. 1. (a) Variation of timing differences between the leading edges of front and back channels as a function of detector operating temperature. (b) Time-delay histogram for ≈ 500 events obtained for $T_c - T \approx 13$ mK. (c) Detector geometry for the F/B experiment.

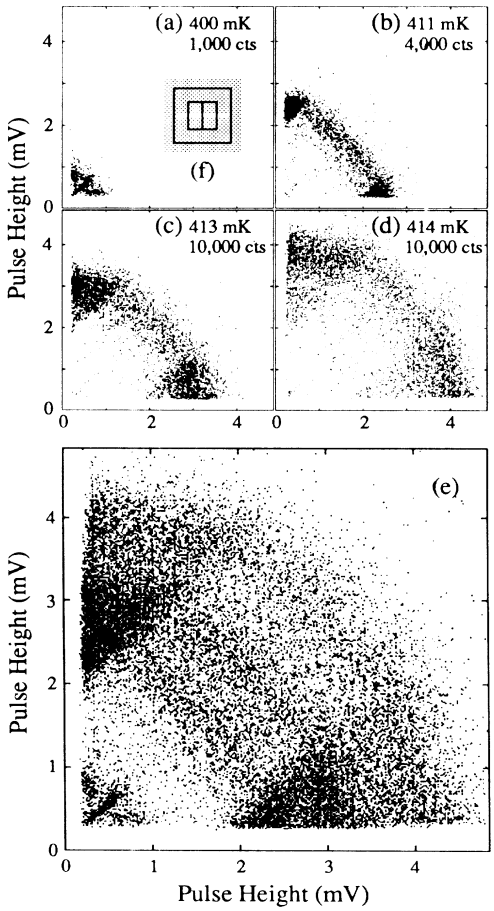

FIG. 2. Coincidence pulse-height distributions obtained with adjacent back-side sensors operated at (a) 400, (b) 411, (c) 413, and (d) 414 mK. (e) Superposition of (a)–(d). (f) Detector geometry for the F/F and B/B experiments.

is due to the α energy spectrum incident on the silicon which has a 15% FWHM peak produced by the gold encapsulation of the ^{241}Am source, and a long, low-energy tail caused by events which fully penetrate the edges of the collimator. The curvature seen in the bands at the higher temperatures results from the electronic distortion discussed above. The location of the high-density regions in these plots is independent of temperature and reflects the temperature-invariant spatial distribution of focused phonons arriving at the surface of the detector. The location of each feature is temperature independent because there exists an exact equivalence between scanning the energy of the α particles and scanning the film threshold by varying the temperature, as discussed below.

Figure 3 shows the temperature dependence of coincidence pulse-height distributions obtained using a detector instrument in the F/F geometry. In Fig. 3(a), the single band of reasonably constant density appears as a result of uniform illumination by the α source and is evidence for good-film homogeneity across the sensors. Figure 3(b) was obtained by measuring the pulse heights of coincident F/F signals while slowly ramping the temperature from 390 to 414 mK. In comparison to the B/B data, the absence of an additional structure in the F/F distributions is striking and largely results from the relatively short α interaction depth. Although very small focusing features must exist on the front surface, they are entirely washed out by the high density of scattered phonons which exceed the film threshold even at our lowest operating temperature. These scattered phonons account for the larger signals observed in the front-side detectors compared to those observed on the back side at the same operating temperature. In Fig. 3, the gaps

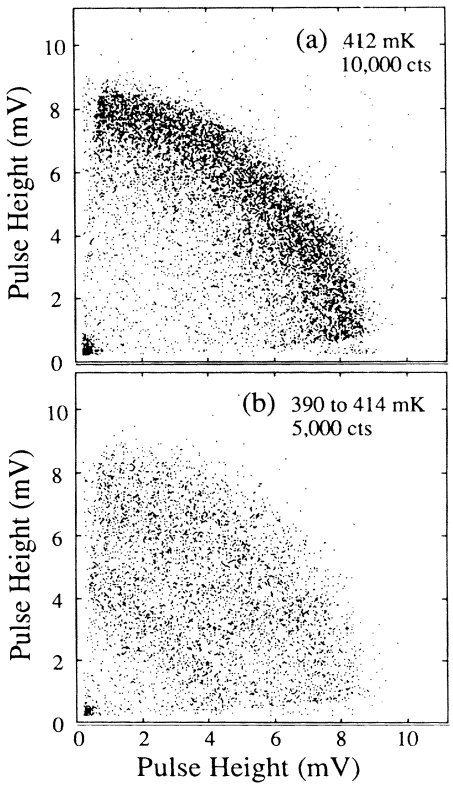

FIG. 3. Temperature variation of coincidence pulse-height distributions obtained with adjacent front-side sensors (a) operated at 412 mK and (b) ramped continuously from 390 to 414 mK.

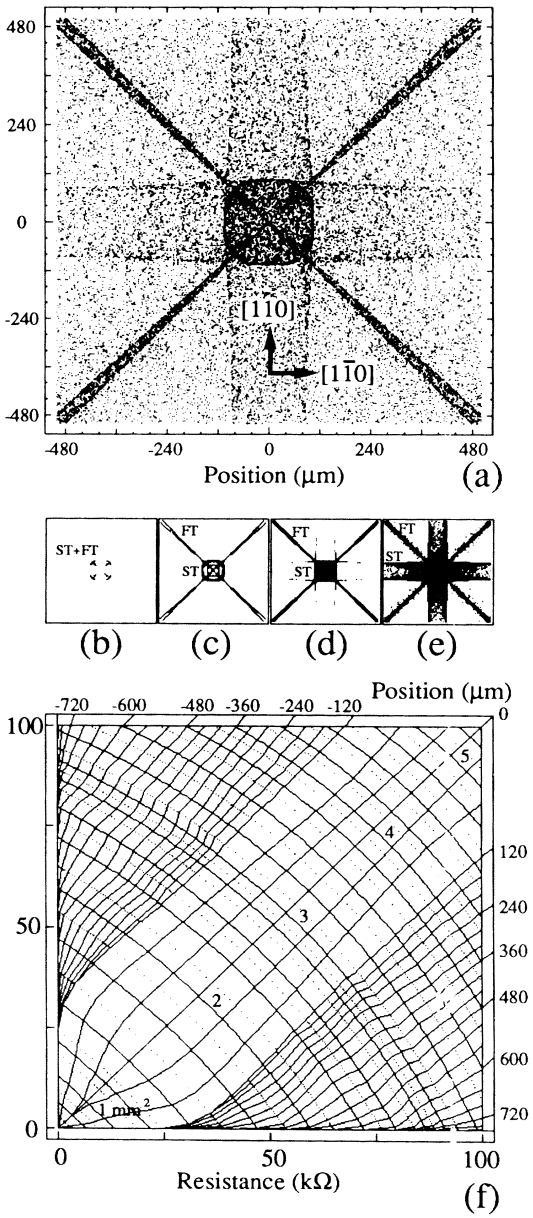

FIG. 4. Monte Carlo calculations showing (a) the energy-density pattern on the (100) face of silicon resulting from purely ballistic transport. Regions exceedings E_σ for thresholds of (b) 2.5, (c) 2, (d) 1, and (e) 0.5 eV/μm^2. (f) Calculated response to the distribution shown in (a) for B/B sensors operated over a range of energy thresholds.

which open along the axes above the threshold cuts for large signals are consistent with α events for which portions of the incident phonon energy are not contained within the 4×4-mm^2 total sensor area.

We can understand the data of Fig. 2 based on a model of ballistic-phonon propagation. The calculated energy-density profile of ballistic phonons striking the (100) surface of Si is shown in Fig. 4(a), for a pointlike event occurring 1 mm from the crystal surface. For a given source energy and operating temperature, we first determine the portion of the energy-density pattern which exceeds threshold E_σ, as shown in Figs. 4(b)–4(e) at four different operating temperatures. Then, for a particular sensor threshold, source energy, and source position, we calculate the pulse heights in the two adjacent sensors by integrating the total area of each sensor exceeding threshold. [The boundary between the sensors is always parallel to the y axis in Figs. 4(a)–4(e).] Finally, using an array of thresholds and source positions, we generate a calculated two-dimensional pulse-height distribution [Fig. 4(f)]. The nearly radial lines correspond to B/B coincidence events for which the centers of the resulting normal regions are equidistant from the boundary between the two sensors. The azimuthal lines represent equal intervals of a parameter $e=fE_0/E_\sigma$, where E_0 is the α-particle energy and E_σ is the critical energy density defined above. The dimensionless attenuation coefficient $f=f_1f_2f_3\approx0.5$ is determined by effects occurring within a ≈1-μsec interval and includes the fraction (f_1) of E_0 which goes directly into phonons, the fraction (f_2) of the total phonon energy which hits the back surface, and the fraction (f_3) of incident phonons which get absorbed into the Ti film. There is good qualitative agreement between Fig. 2 and Fig. 4(f). These calculations identify both the energy and position of each α event in Fig. 2, so that the detector is a position-sensitive spectrometer.

The Monte Carlo distributions of Fig. 4 also aid our understanding of the features observed in the B/B pulse-height distributions (Fig. 2). The radial band at low pulse heights corresponds to equal partitioning of energy in the adjacent sensors and is due to the four normal areas [ST (slow transverse) and FT (fast transverse) phonons] shown in Fig. 4(b) for high thresholds. These data points correspond to event positions for which two of the four small areas lie on either side of the boundary between the sensors. At lower thresholds (higher operating temperatures) this radial band disappears, and symmetric triangular regions begin to dominate the pulse-height distribution. These triangular regions result from an array of phonon-energy-density patterns, such as those shown in Figs. 4(c)–4(e). For these, when the boundary between the sensors lies within the central spot (ST and FT phonons) the partitioning of area between sensors varies rapidly as a function of position, whereas when the boundary lies to either side of the large central spot the partitioning is less sensitive to position.

We conclude, after an analysis of both the F/B time-delay data and the geometric B/B pulse-height distribution data,[14] that approximately one-third of the phonon energy absorbed in the back-side sensors within the initial ≈0.5 to 1 μsec arrives ballistically. In addition, the F/F signals are larger than the B/B signals at every operating temperature, and are dominated by a phonon energy which has been isotope scattered from the bulk or reflected from the back surface onto the front surface of the detector. We note that phonon down-conversion to below about 1.25 THz is necessary to produce a mean free path for isotope scattering greater than 1 mm, and must caution that this down-conversion may not occur in the local α interaction region within the crystal, but rather at the crystal surface which is within ≈25 μm of the α track, and 40% covered with titanium. Further experiments with x rays and neutrons which interact deep in the crystal are expected to resolve this down-conversion ambiguity.

We thank B. Neuhauser, J. McVittie, and G. Feigl for technical aid and B. Dougherty and K. Irwin for useful discussions. This work is funded in part by DOE Grant No. DE-AM03-76-SF00-326.

[1]See, for example, *Nonequilibrium Phonon Dynamics,* edited by W. E. Bron, NATO Advanced Study Institutes, Ser. B, Vol. 124 (Plenum, New York, 1985).

[2]G. A. Northrop and J. P. Wolfe, Phys. Rev. B **22**, 6196 (1980).

[3]See, for example, G. F. Knoll, *Radiation Detection and Measurement* (Wiley, New York, 1979).

[4]B. Sadoulet *et al.*, in "PHONONS 89" (World Scientific, Singapore, to be published).

[5]B. Neuhauser, B. Cabrera, C. J. Martoff, and B. A. Young, Jpn. J. Appl. Phys. **26**, 1671 (1987).

[6]B. A. Young, B. Cabrera, and A. T. Lee, in "Low Temperature Detectors for Neutrinos and Dark Matter III," edited by L. Brogiato, D. V. Camin, and E. Fiorini (Editions Frontiere, Gif-sur-Yvette, to be published).

[7]F. Pröbst *et al.*, Nucl. Instrum. Methods Phys. Res., Sect. A **280**, 251 (1989).

[8]B. Cabrera (to be published).

[9]The intrinsic Si wafer substrates (>1500-Ω resistivity) were produced at Unisil Corp. (Mountain View, CA) using the magnetic Czochralski technique.

[10]E. S. Yaney *et al.*, IEEE Trans. Electron Devices **26**, 10 (1979).

[11]A. T. Lee, Rev. Sci. Instrum. **60**, 3315 (1989).

[12]B. Neuhauser *et al.* (to be published).

[13]Temperatures were measured with a Lake Shore Ge thermometer and changes are correct to several tenths of mK, although the absolute transition temperature is only known to tens of mK.

[14]B. A. Young, B. Cabrera, and A. T. Lee (to be published).

[15]See, for example, M. Tinkham, *Introduction to Superconductivity* (McGraw-Hill, New York, 1975).

[16]H. J. Maris, Brown University report, 1989 (to be published).

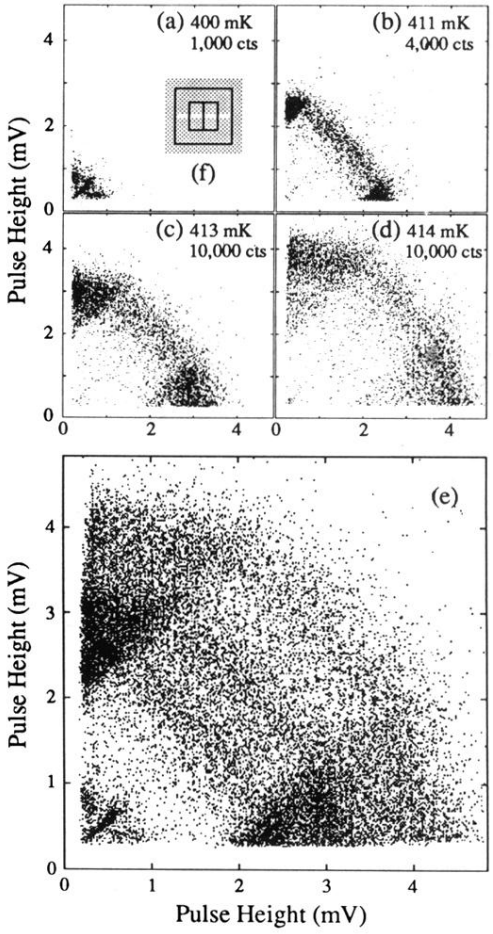

FIG. 2. Coincidence pulse-height distributions obtained with adjacent back-side sensors operated at (a) 400, (b) 411, (c) 413, and (d) 414 mK. (e) Superposition of (a)–(d). (f) Detector geometry for the F/F and B/B experiments.